Appl Phys B (2011) 102: 529–538
DOI 10.1007/s00340-011-4411-9

Applied Physics B
Lasers and Optics

Injection-locked single-frequency laser with an output power of 220 W

L. Winkelmann · O. Puncken · R. Kluzik · C. Veltkamp · P. Kwee · J. Poeld · C. Bogan · B. Willke · M. Frede · J. Neumann · P. Wessels · D. Kracht

Received: 9 July 2010 / Revised version: 1 October 2010 / Published online: 11 February 2011

Abstract A solid-state laser system for the next generation of gravitational wave detectors with an output power of 220 W at the wavelength of 1064 nm is presented. Single-frequency operation of the laser was achieved by injection-locking of a high-power ring oscillator to an amplified non-planar ring oscillator (NPRO) following the Pound–Drever–Hall scheme. The high-power stage which features four longitudinally pumped Nd:YAG laser crystals as active media in a ring resonator configuration was designed for reliable long term operation. Using a non-confocal ring cavity to filter the output beam, a pure TEM_{00} mode with 168 W output power was obtained.

1 Introduction

The most promising approach to detect gravitational waves on Earth is based on large scale Michelson interferometers, which perform high precision differential length measurements. The largest detectors of this kind are the Laser Interferometer Gravitational Wave Observatories (LIGO) in the USA [1]. Two of these detectors (with 4 and 2 km arm length) are merged in one observatory located at Hanford, Washington. The third observatory was built near Livingston, Louisiana, and contains a 4 km Michelson interferometer. Both observatories inherit the highest sensitivity of today's gravitational wave detectors and can achieve a detection range of more than 30 Mpc for inspiral neutron stars [2]. A key factor for improvement of the sensitivity is to reduce noise sources, which directly couple into the detection signal. One limitation for today's LIGO detectors is the shot noise. As the shot noise limited sensitivity scales proportionally with the inverse square root of the optical power inside the interferometer, the sensitivity would strongly benefit from a power increase of the laser light source [1]. Besides the need of a high output power, the light source has to fulfill stringent requirements for beam profile, pointing, amplitude and frequency noise not to induce additional noise into the gravitational wave channel [3].

Currently, two 35 W amplifier systems, developed by Frede et al. [4], are installed at the LIGO sites for the 4 km interferometer and have proven to be well suited as a light source for an interferometric gravitational wave detector. For the next major upgrade of the LIGO detectors—advanced LIGO—an output power increase to a level of more than 165 W in a pure Gaussian beam is desired [5]. To fulfill this requirement, a high-power oscillator, which can be injection-locked to the existing 35 W amplifier system, was realized. In the following sections, the optical and mechanical setup of the high-power oscillator and the system performance are presented.

2 Laser concept

The laser development leading to the laser system for advanced LIGO described in this paper has been carried out

L. Winkelmann (✉) · O. Puncken · R. Kluzik · C. Veltkamp · M. Frede · J. Neumann · P. Wessels · D. Kracht
Laser Zentrum Hannover e.V., Hollerithallee 8, 30419 Hannover, Germany
e-mail: l.winkelmann@lzh.de

P. Kwee · J. Poeld · C. Bogan · B. Willke
Max-Planck-Institut für Gravitationsphysik (Albert-Einstein-Institut) und Leibniz Universität Hannover, Callinstr. 38, 30167 Hannover, Germany

B. Willke · J. Neumann · P. Wessels · D. Kracht
Centre for Quantum-Engineering and Space-Time Research—QUEST, Welfengarten 1, 30167 Hannover, Germany

over several stages. The fundamentals have been derived by Frede et al. in preliminary experiments. With a first injection-locked two head laser system, a single-frequency output power of 87 W could be achieved [6]. The feasibility of power scaling by doubling the number of laser crystals was demonstrated in a first four head prototype laser with a diffraction limited output beam and an output power of 213 W, but without injection-locking [7]. In the migration from this prototype laser to the final injection-locked laser system presented here, several improvements, which will be described in the following sections, have been realized in order to make the system more robust and reliable for long term operation in terms of beam quality, output power and injection-locking behavior.

For this laser system, an identical version of the 35 W amplifier, which is already operated at two LIGO sites, was used as seed laser. As sketched in the system schematic of the laser in Fig. 1, a 2 W non-planar ring oscillator (NPRO, manufactured by InnoLight) is amplified in a single pass through four longitudinally pumped Nd:YVO_4 crystals (details can be found in [4]). The single frequency beam from the amplifier is then fed into the main oscillator, which consists of four end-pumped Nd:YAG crystals arranged in a ring resonator. This resonator has got an asymmetric structure for selective higher order mode discrimination and features a piezo-actuated mirror for active length control. Both systems are optically decoupled by a Faraday isolator specifically designed for high power levels [8]. To injection-lock the high-power oscillator following the Pound–Drever–Hall scheme [9], an EOM was placed between NPRO and power amplifier.

In the following section, the optical configuration of the high-power oscillator will be presented in detail.

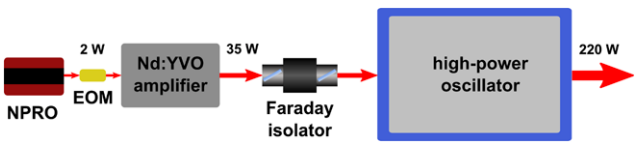

Fig. 1 Schematic setup of the injection-locked laser system for advanced LIGO

2.1 Optical setup

To achieve high linearly polarized output power levels and good beam quality, a longitudinally pumped laser design was chosen. The presented laser features four Nd:YAG crystals for a reduction of heat load in each active media compared to a single crystal design. Each laser crystal is pumped by seven fiber coupled diode lasers with a combined maximum output power of 315 W (7 × 45 W). The seven attached 400 µm multimode fibers are combined into a single fiber bundle with polished bare-end tips. To avoid hot spots due to the non-uniformity of the pump light distribution, the light from the fiber bundle is homogenized by propagating through a 100 mm long and 2 mm in diameter fused silica rod. Due to total internal reflection inside the glass rod, the pump light is mixed, resulting in a parabolic intensity profile measured at the exit pupil.

As shown in Fig. 2, the tip of the glass rod is imaged with two lenses through the end facet of the laser crystal forming a focus with the imaging plane approx. 10 mm inside the rod. Two undoped 7 mm long end-caps at both ends of the laser crystal prevent bulging of the end facets due to thermal stress and enable efficient water cooling of the pumped region. The total length of the laser crystal is 54 mm and it has a diameter of 3 mm. A low Nd^{3+} doping concentration of 0.1 at.% in combination with a pump light double pass was chosen. This combination ensures that more than 90% of the pump light is absorbed at a center wavelength of 808 nm and a FWHM of 2.5 nm. Furthermore, the axial uniformity is higher compared to a 0.2 at.% doped crystal in a single pass configuration. This allows for higher pump power before the thermally induced fracture of the laser rod occurs [10]. Each laser crystal is pumped at power levels up to 250 W. To actively cool the crystal, a turbulent jet of water flows directly around its barrel surface. Because of the refractive index difference between 1.82 for Nd:YAG and 1.33 for water, this design provides a pump light guidance inside the laser rod due to total internal reflection.

2.2 Thermal lensing

In longitudinally-pumped laser rods, the heat produced by the absorbed pump light forms a non-uniform temperature

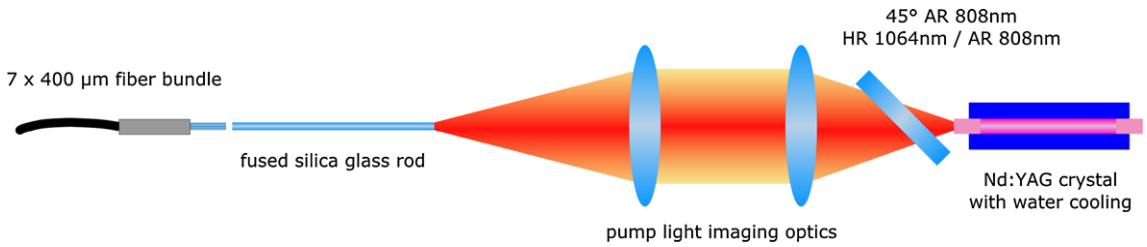

Fig. 2 Laser head optical setup

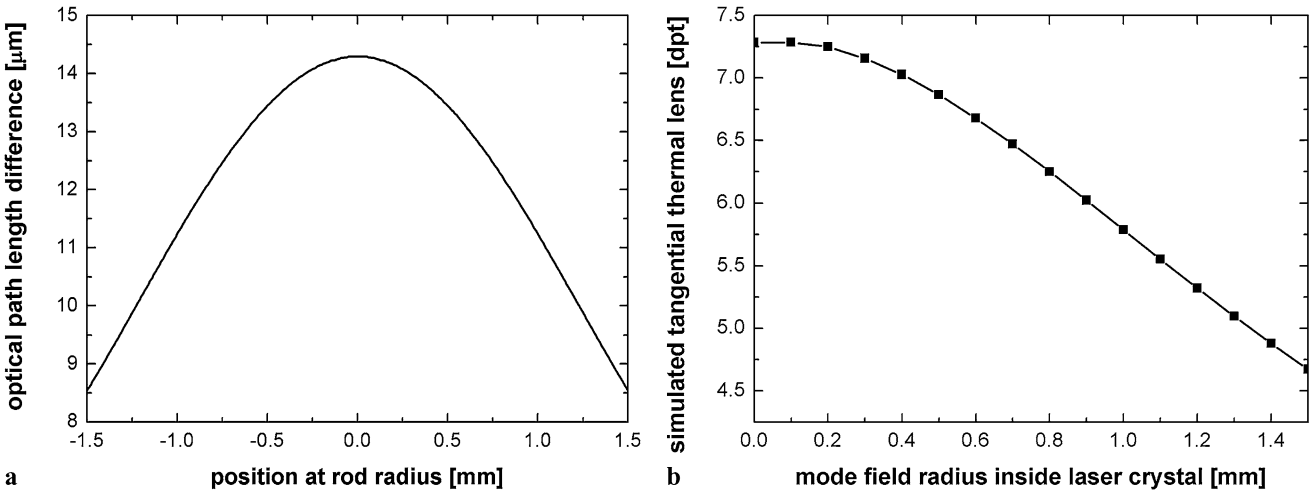

Fig. 3 (**a**) Resulting optical path length difference from the numerical simulation at an incident pump power of 250 W at a center wavelength of 808 nm with a FWHM of 3 nm. (**b**) Refractive powers derived from numerical simulation for different beam radii

distribution inside the active media. Solving the stationary heat equation, this temperature profile can be calculated as a function of the injected pump power, the pump light distribution, the doping concentration, and the pump wavelength. The temperature gradient inside the active area of the laser crystal during optical pumping results in a thermally induced non-uniform refractive index change of the Nd:YAG material leading to thermal lensing. By integrating the resulting optical path length difference over the full length of the crystal, a thermal lens profile depending on the parameters given above can be deduced. Since the thermal conductivity decreases with decreasing temperatures, the laser-rod was cooled with the lowest possible water temperature of 18°C at the given ambient conditions. Lower water temperatures would result in condensing moisture at the cooled structure. Thus, the heat load, which is concentrated in the center of the laser crystal, is more efficiently transferred to the outer wall of the rod and then removed by the constant water flow.

Even though the laser crystals are pumped with a parabolic intensity profile, the resulting thermal lens does not have the parabolic shape of an ideal lens. The effective thermal lens can then be approximated by a parabolic fit of the refractive index profile over the incident laser beam radius and does vary with beam size. In Fig. 3, it is shown that the effective thermal lens decreases with increasing beam size.

We calculated this thermal lensing effect inside the laser crystal by varying pump power and laser mode size while keeping all other parameters fixed, and could derive a numerical approximation for the thermal lens with respect to these two parameters. This function $f(r, P)$, where f is the focal length, r the laser mode radius at the principal plane of the lens and P the incident pump power, is used for all four crystals in an ABCD matrix calculation [11, 12] of the high-power oscillator resonator (see the next section for resonator details).

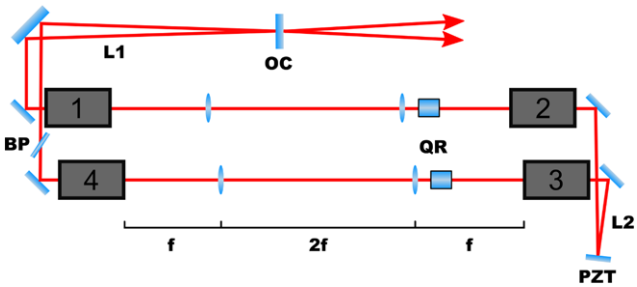

Fig. 4 Schematic of the asymmetric resonator with four laser heads (No. 1–4), 90° polarization rotating quartz rotator (QR), output coupling mirror (OC), uncoated Brewster plate (BP), piezo-actuated mirror (PZT), long arm length (L1) and short arm length (L2)

2.3 Resonator design

To scale the output power while keeping thermal effects and therefore the beam quality in a adequate range, a ring resonator as sketched in Fig. 4 with four laser crystals was designed. On the right hand side of the cavity (L2), a highly reflective mirror mounted on a piezo actuator was installed for an active resonator length control during injection-locking. On the other side of the cavity (L1), the long beam path to the output coupling mirror was folded by a 45° HR mirror and a plane-parallel glass substrate was placed in Brewster angle inside the resonator to maintain linear polarization. In order to compensate the thermally induced birefringence, two laser head modules are aligned opposing each other on one optical axis and a standard depolarization compensation with a 90° polarization rotating quartz crystal (QR) and a setup to image the principal planes of the thermal lenses onto each other is used [13].

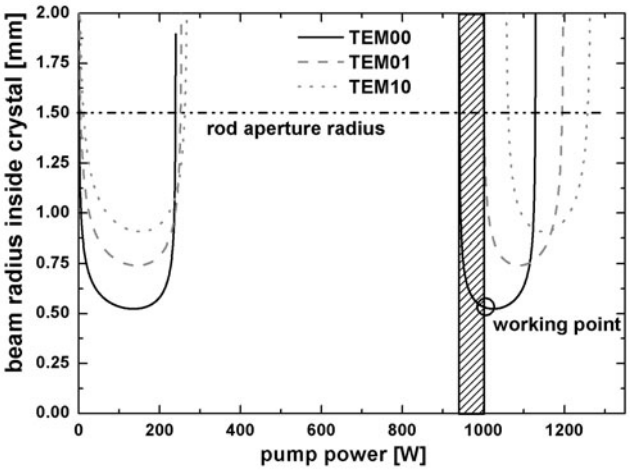

Fig. 5 Mode size inside the laser crystals with respect to incident pump power for different transverse modes

As explained in the previous section, the effective thermal lens depends strongly on the laser beam diameter. To take full advantage of this effect, the resonator of the high-power oscillator is set up as an asymmetric cavity. In such a cavity, the stability range is split into two separated stable areas with respect to pump power [12]. With the thermal lens derived from the model described in the previous section, the beam radius in the resonator was calculated by determining a self consistent solution for beam size and corresponding thermal lens. This procedure was repeated for different higher order modes with correspondingly larger beam diameters inside the laser crystals (dashed/dotted lines in Fig. 5). Due to their larger mode diameter, these higher order modes (in this case Gauss–Laguerre modes) see a lower thermal lens. Thus, their stable operation point is shifted to higher total pump powers. For us, the first stability range shown in Fig. 5 is of no interest, because it refers to very low pump powers of less than 250 W total pump power cumulated of all laser heads. The second stability range with a threshold at approx. 900 W of combined pump power was chosen for the operation of the high-power oscillator.

Contrary to that the TEM_{00} mode experiences the largest thermal lens compared to all higher order transversal modes, as it has got the smallest beam diameter of all resonator modes. Hence, the TEM_{00} mode is the first and only resonator mode that can stably oscillate inside the asymmetric laser cavity at the second stability range threshold. The pump power region, in which solely a fundamental mode operation can be achieved, is shown as shaded area in Fig. 5. Higher order modes, which have smaller thermal lenses because of their larger mode field diameter, need higher pump power levels for stable operation. An optimal operation point for the fundamental mode is found when the beam size of the TEM_{00} mode inside the resonator has the lowest supported value and the threshold for the oscillation of a higher order mode is not exceeded. At this point, the pump power induced beam size variations in the high-power ring oscillator are reduced to a minimum.

The position of the second stability range with respect to the incident pump power can be altered by the short arm length of the asymmetric resonator (L2 in Fig. 4). A reduction in length shifts the fundamental mode operation point to higher pump power. This length defines the upper pump power limit for a stable TEM_{00} mode operation of the oscillator to be approx. 275 W per laser head. To account for aging of the InGa:As diode lasers used for pumping, the overall output power per laser head was reduced to 250 W. The derated operation at 80% of the diode lasers maximum output power capability should significantly increase their lifetime, which is specified with $> 20{,}000$ h at full output power by the manufacturer.

The beam radius inside the four laser rods scales with the length of the long arm of the resonator (L1 in Fig. 4) located at the side of the output coupling mirror. Longer distances of the output coupling mirror from the first and fourth laser crystals increase the TEM_{00} radius at the fundamental mode working point. Optimization of this arm length of the asymmetric cavity mainly affects the overlap of pump mode and laser mode and thus maximizes the efficiency and output power. The length of the long arm was optimized for a pump power level of 250 W per crystal.

2.4 Injection-locking

For single-frequency operation of the laser, the high-power oscillator was injection-locked to the 35 W amplifier system (Fig. 1). To adapt the length of the oscillator's cavity and hence its resonance frequency to the seed frequency, the reflecting mirror of the short arm length L2 was mounted on a piezo actuator (PZT). To avoid mechanical vibrations introduced by the piezo actuator motion, a second identical actuator was glued on the opposite side of the mirror mount. Both piezo actuators are connected in parallel to the high-voltage driver and move in opposite directions. Hence, all mechanical forces applied to the mirror mount by one of the piezo actuators are compensated by the movement of the counter-working one. The first resonance of the piezo-actuated mirror including the glass substrate was at 35.5 kHz, which could be suppressed by an electronic notch filter in the feedback loop.

In order to generate phase-modulation sidebands needed for the Pound–Drever–Hall locking scheme an EOM was installed between the NPRO and the amplifier stage (Fig. 1). A typical error signal obtained by ramping the piezo mirror is shown in Fig. 6. The maximum achieved unity gain frequency of the injection-locking control loop was 22 kHz. An automatic lock acquisition system required typically less than 10 ms to bring the laser system into the injection-locked state.

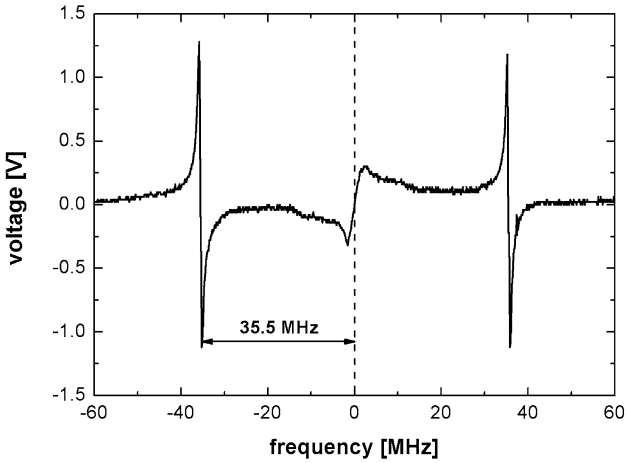

Fig. 6 Error signal at a modulation frequency of 35.5 MHz for the generation of sidebands

Without seed laser, the oscillator delivered a summarized fundamental mode output power of 175 W in bidirectional operation. Being injection-locked by the 35 W amplifier, the single-frequency output power of the combined system increased to 220 W. The discrepancy in the injection-locked case to the sum of both laser powers which is expected in theory can be explained by the reflectivity of the output coupling mirror, which is optimized for the locked state and not for the free running laser operation. An optimum transmission of this output coupling mirror was experimentally determined using a set of substrates with different reflectivity around 50%.

3 Mechanical setup

During the design phase of the laser system for Advanced LIGO, the increase of output power to a level above 200 W with low power in higher order modes and merging of all necessary components in one compact setup was the main goal. Additionally, the system had to be easily maintainable, as well as reliable and stable over a long time period.

As mentioned above, the high-power oscillator consists of four laser heads (see Fig. 2). Each laser head is equipped with a water-cooled pump-chamber, storing one Nd:YAG crystal. The water inside the chamber flows directly around the polished rod surface. In standard cooling chamber designs, the water is injected through the nozzles at each laser crystal tip pointing onto the rod's surface and ejected after passing through a tube surrounding the crystal barrel. Pressure fluctuations of the water jet hitting the laser crystal induce mechanical vibrations into the active media and introduce additional noise into the laser output beam. To reduce the mechanical vibrations coupled into the rod, a circular flow chamber was developed, from which the water is guided turbulently into the flow tube of the cooling chamber. An identical structure was applied to the end of the pump chamber for the water outlet. Finite element method (FEM) simulations combined with a computational fluid dynamics (CFD) analysis of this pump chamber design showed that the injection of water in the direction opposite to the incident pump light leads to a more homogeneous axial temperature distribution inside the laser crystal compared with co-linear cooling schemes.

The heat load on the opto-mechanical components of the laser head shown in Fig. 7 is mainly generated by the pump light and not by the laser beam itself. Approximately 5 W of the optical power emitted out of the fiber bundle tip are not coupled into the homogenizer. This optical power gets absorbed and heats up the back of the homogenizer mount. After the light has passed the pump light imaging lenses, 2.5% of its optical power is reflected at the dichroic mirror in front of the pump chamber onto a water cooled copper beam block. Because of the pump light double pass in the laser crystals, the non-absorbed pump power is propagating backwards in direction of the pump optics. The maximum achievable absorption of the laser crystals used in this laser system is approx. 90% at a center wavelength of 808 nm and an FWHM of 2.5 nm. After passing the pump light imaging optics, approx. 15 W of optical power illuminate the tip of the homogenizer holder. The remaining power, approx. 5 W, passes through the homogenizer and is partially absorbed by the fiber bundle ferrule and its mount. An additional source for temperature induced misalignment of opto-mechanical components is the fluorescence of the laser crystal when it is pumped. Approximately 5 W of spontaneous emission leak out of each end facet of the laser crystal. The light which

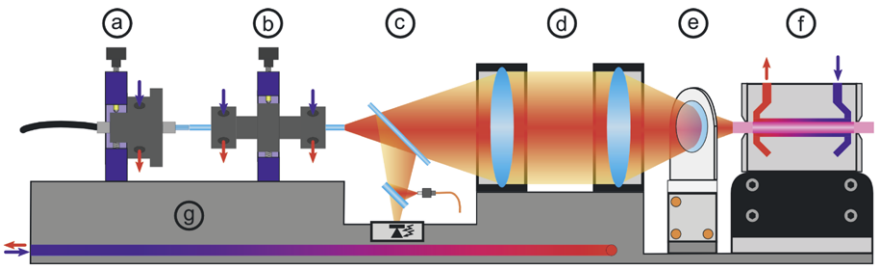

Fig. 7 Optical setup of the laser head components: (**a**) fiber bundle holder, (**b**) homogenizer holder, (**c**) pump light diagnostic for power and wavelength control, (**d**) pump light imaging optic, (**e**) adjustable dichroic resonator mirror, (**f**) pump-chamber with Nd^{3+}:YAG crystal, and (**g**) optical bench

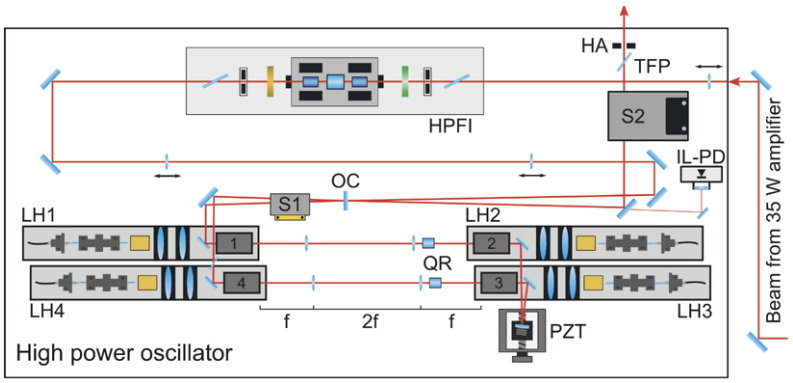

Fig. 8 Schematic setup of the injection-locked high-power laser system with: laser head 1–4 as described in Fig. 7 (LH1–4), output coupling mirror (OC), piezo-actuated mirror with linear stage (PZT), 90° quartz rotator (QR), high-power Faraday isolator (HPFI), injection-locking photo diode (IL-PD), shutter 1 and 2 (S1, S2), thin film polarizer (TFP), and halo aperture (HA)

is emitted in the direction of the depolarization compensation is blocked by a water cooled beam block with an aperture for the resonator internal laser beam of 5 mm in diameter. Unfortunately, the light emitted in the direction of the dichroic mirror cannot be blocked by a water cooled aperture because of spatial limitations at this position. To reduce the heat load on the mirror mount itself, a very thin structure of the machinable ceramic MACOR was used to hold the mirror and to connect it to an adjustable mount. The mirror mount itself is placed far enough below the crystal end facet and hence is not affected by the fluorescence emitted during laser pumping. This solution is advantageous as MACOR is partially transmissive for laser radiation at 808 nm wavelength.

To compensate for the thermally induced elongation and hence misalignment of the mentioned opto-mechanical components, all areas where heat is introduced into the structure are water cooled or shielded by water cooled copper heat sinks. Additionally, the optical bench of all laser heads is temperature stabilized by direct water cooling.

Even though the diode laser's currents are derated by 20% to achieve a longer lifetime, the emitted power level will constantly drop over time due to aging. Because of the lower efficiency for aged diode lasers, the temperatures inside the diode bars will rise as well, and subsequently, the emission spectrum will shift to longer wavelengths. For long term operation of the laser system, both effects have to be regularly compensated for. Consequently, the pump light power and spectrum have to be monitored for each laser head. For this purpose, a small fraction of the pump light is picked up by a 45° AR-coated substrate. The divergent beam is focused by two lenses (not shown in Fig. 7) through a 90/10 beam splitter. The reflected part of the beam, which contains 90% of the power, is directed onto a 62.5 µm gradient index multimode fiber for spectral analysis. The four fibers of the individual laser heads are connected to a 4×1 multimode switch whose output is analyzed by an optical CCD grating spectrometer. For pump power monitoring, the transmitted beam is detected by a large diameter silicon photodetector. Both devices are read out by analog-to-digital converters connected to a Stored Program Control unit. All values are monitored and stored constantly. Although in principle an automated compensation should be feasible, this has not been implemented, yet, because diode degradation is a slow process.

Inside the high-power oscillator box, whose optical layout can be seen in Fig. 8, a birefringence and thermal lens compensated Faraday isolator was integrated to shield the 35 W amplifier from the backward propagating light of the ring oscillator [8]. Furthermore, two safety shutters and diagnostic photo-diodes at different positions for an online characterization of the system performance have been included.

All parameters of the complete laser system, e.g., diode laser temperatures and currents, piezo actuator voltage and all photodiode signals are monitored, logged and controlled by a Stored Program Control.

4 Resonator thermal elongation compensation

Two different sources for the thermally induced elongation of the laser resonator can be found. The first is the ambient temperature in the laser room. In the laser design, we assumed room temperature variations of 3 K peak-to-peak over one year. Due to the water cooled structures, the temperature change inside the laser box is lower than outside. As seen in Fig. 9(a) and 9(b), when the room temperature was changed from 22.5°C to 25°C, the air temperature inside the box increased by only 0.6°C.

As described above, the resonance frequency of the high-power oscillator is controlled by a fast piezo actuator for the injection-locking. This piezo actuator has a range of approx. 4 µm at 375 V of driving voltage. The resonator length of the oscillator is about 1.8 m, resulting in a temperature induced lengthening of 19 µm/°C due to the expansion of the base-plate (stainless steel ISO 1.4313). Furthermore, atmospheric pressure and air temperature fluctuations change the refractive index of the air inside the laser box, which in turn change the optical path length inside the resonator (0.45 µm/hPa and −1.4 µm/°C). All effects are of the order

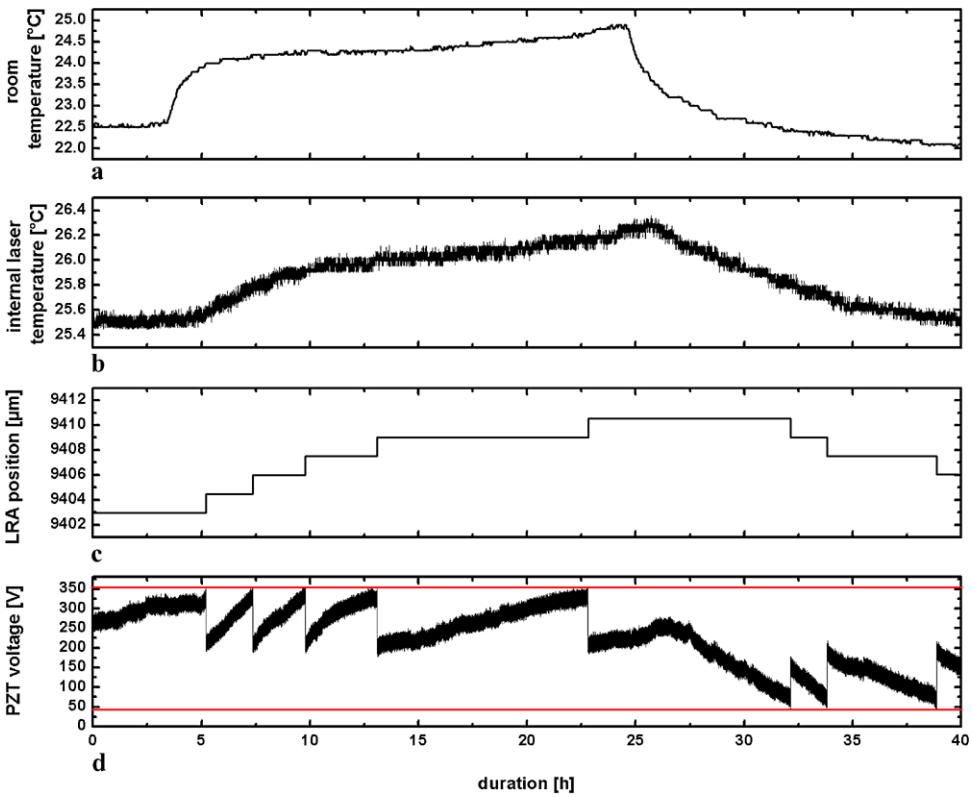

Fig. 9 Induced room temperature change to test the long range actuator performance: (**a**) room temperature measured above optical table, (**b**) temperature inside laser housing, (**c**) position of long range actuator, and (**d**) control voltage for resonator internal piezo mirror

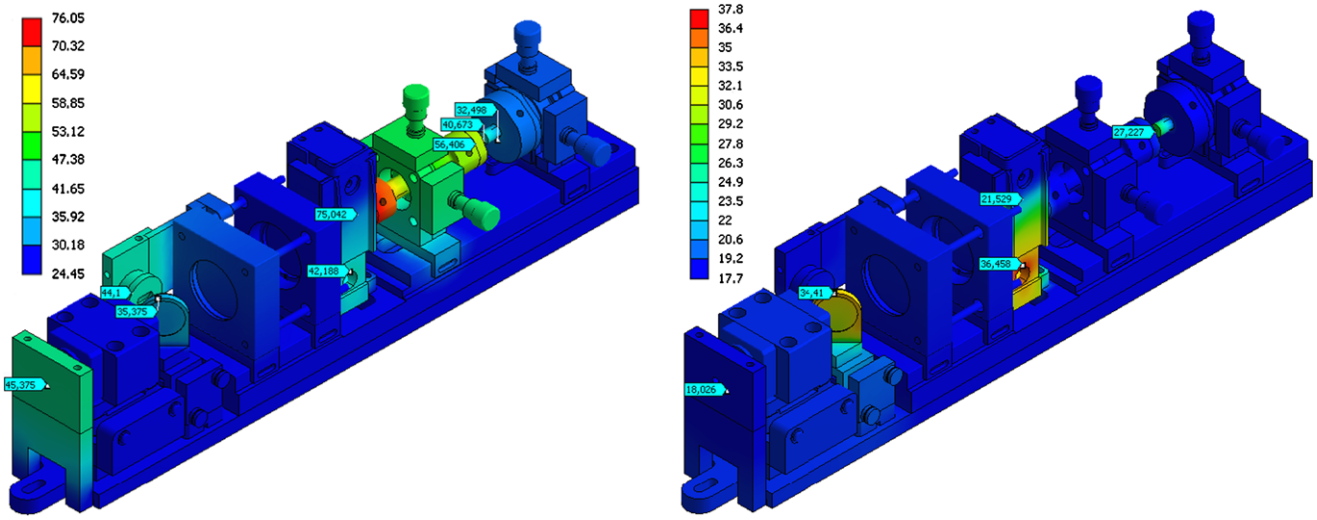

Fig. 10 (*Left*) FEM simulation without water cooling of the laser head with heat loads as specified in Sect. 3. (*Right*) FEM analysis of the same model with water cooling of the opto-mechanical parts. To simplify the model, a constant water temperature of 18°C neglecting the water temperature gradient (approx. < 1 K for a flow rate of 0.5 l/min for each individual laser head) due to heating is assumed

of several tens of micrometers, which cannot be compensated by the piezo actuator.

The second source for resonator length changes is the heat load generated in the mechanical components by absorbed laser or pump light. As described in Sect. 3, the internal heat removal has been improved to a maximum by water cooling in order to keep the temperature of the mechanical structure low. In comparison with previous, uncooled prototypes of the laser system, the maximum temperatures of critical opto-mechanical components were reduced from over 80°C to less than 40°C. To further investigate this reduction of temperature in the mechanical structure, an FEM analysis with the commercial software ANSYS was performed. The derived results presented in Fig. 10 indicate a

sufficient reduction of the temperatures of all optical components with a high heat load under water cooled condition. These simulations have been verified by a measurement with a thermo-optical camera. Comparing analysis and measurement, a good agreement for the derived temperatures with a deviation of less than 0.5°C was found.

In order to compensate for the length variations induced by temperature and pressure changes, the mirror mount carrying the piezo actuator was attached to a slowly moving linear stage with a DC motor. This stage is able to move with a maximum resolution of a few nm and has very smooth movement and high mechanical stiffness (Physical Instruments model M126-DG1).

This so-called long range actuator (LRA) is controlled via the software control system. When the piezo driving voltage exceeds a specific upper or lower limit, the LRA performs a pre-defined slow step to bring the piezo actuator to its neutral position at approx. 180 V. The length of one step can be set inside the software control and is experimentally determined. The step duration is set to 2 seconds. This slow movement is then simultaneously compensated by an identical movement in the opposite direction of the piezo and does not interfere with the injection-locking (see Fig. 9(c) and 9(d)), as all contributing frequency components in the LRA movement are several orders of magnitude below the piezo control loop unity gain frequency.

With this scheme, not only the temperature elongation but also the atmospheric pressure induced distortions of the resonator length can be compensated by the combined action of the LRA and the piezo actuator. In a test run with 40 h duration, the laser was successfully operated without any loss of injection-lock in spite of the room temperature change of about 2.5 K.

5 Laser characterization

In a detailed characterization, the suitability of the laser system as a light source for the next generation of gravitational wave detectors was verified. All tests were performed with the injection-locked, single-frequency laser system. An active stabilization to fulfill the amplitude noise, frequency noise, beam quality and pointing stability requirements for advanced LIGO will be implemented in a next step [5].

5.1 Output power and higher order mode content

The injection-locked laser system delivers an output power of 220 W. Due to the highly aberrated thermal lenses inside the laser crystals, a deviation of the laser's fundamental mode from a perfect TEM_{00} mode is expected. In fact, a halo, which is clearly separated from the central TEM_{00} mode part of the beam, can be identified with a CCD camera. Nevertheless, there is no evidence that this halo is related to any higher order mode oscillating inside the laser cavity.

In interferometric gravitational wave detectors, only the power within the TEM_{00} mode can be used. In order to analyze the fraction of output power in this fundamental Gaussian mode, a degenerate scanning non-confocal ring cavity was used. This cavity is based on the design of the Pre-Mode Cleaner (PMC) developed for the LIGO detector [14]. A small portion of laser light, approx. 130 mW, is picked up after a HR mirror behind the laser's output window and is used to determine all laser output beam parameters. This laser beam is then aligned and mode-matched to the PMC cavity. As the PMC cavity is a non-confocal cavity, the different transversal modes have different eigenfrequencies. The input beam can be decomposed into the eigenmodes of the PMC by scanning the PMC cavity length over one free spectral range and monitoring the transmitted power signal.

Two different characteristic mode scans are shown in Fig. 11. To derive the fraction of power in higher order modes, a numerical fit is performed. From this fit, the power and order of the individual higher order modes are obtained. Unfortunately, the background visible in the mode scan data in Fig. 11(a), which is caused by the halo surrounding the TEM_{00} mode profile, cannot be accurately taken into account by this analysis. For the second measurement (Fig. 11(b)), we removed the halo structure with an external water cooled hard aperture. Approximately 40 W of output power were dumped into the halo aperture, resulting in an output power of 180 W. In this configuration, we measured a mode scan without the background present and a higher order mode content of only 7.5%.

According to the advanced LIGO requirements, the laser output power in the fundamental Gaussian mode has to be more than 165 W with less than 5% of power in higher order modes. To filter out all higher order modes, a PMC optimized for high incident powers is used. Unlike the low power PMC described above, the high-power version is based on a bow-tie resonator configuration to increase the resonator length while keeping the overall size small [15]. Using a second set of Pound–Drever–Hall electronics and re-using the phase modulation side-bands reflected from the high-power oscillator, the filter cavity was locked to the high power beam of the laser. The maximum achieved transmitted power in the TEM_{00} mode was 168 W, which is consistent with the mode scan after the halo aperture.

5.2 Relative power and frequency noise

To reduce the influence of laser power and frequency noise on the gravitational wave detection signal, an active sta-

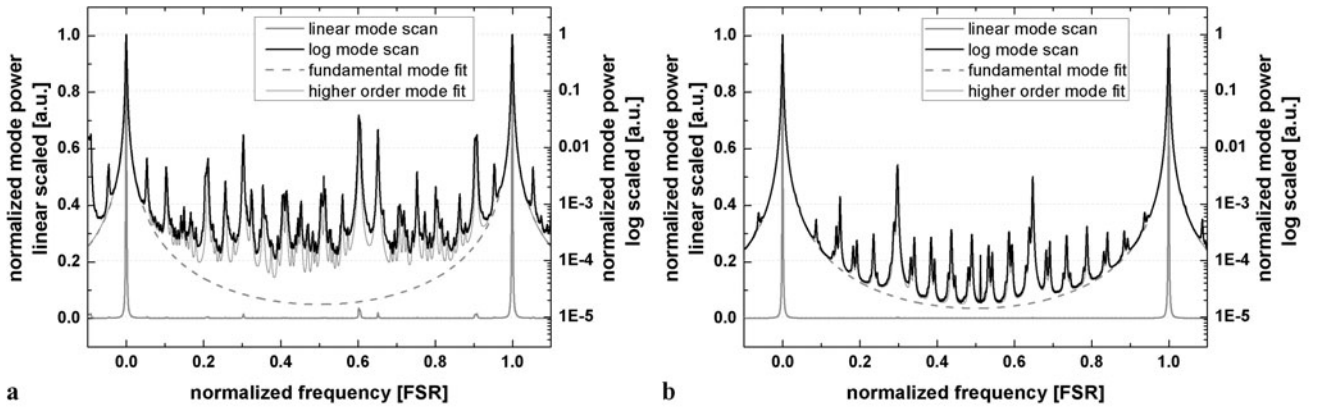

Fig. 11 Transversal mode scan. (**a**) Measured higher order mode content of $< 12\%$ without halo aperture in output beam. (**b**) Higher order mode content $< 7.5\%$ with halo aperture

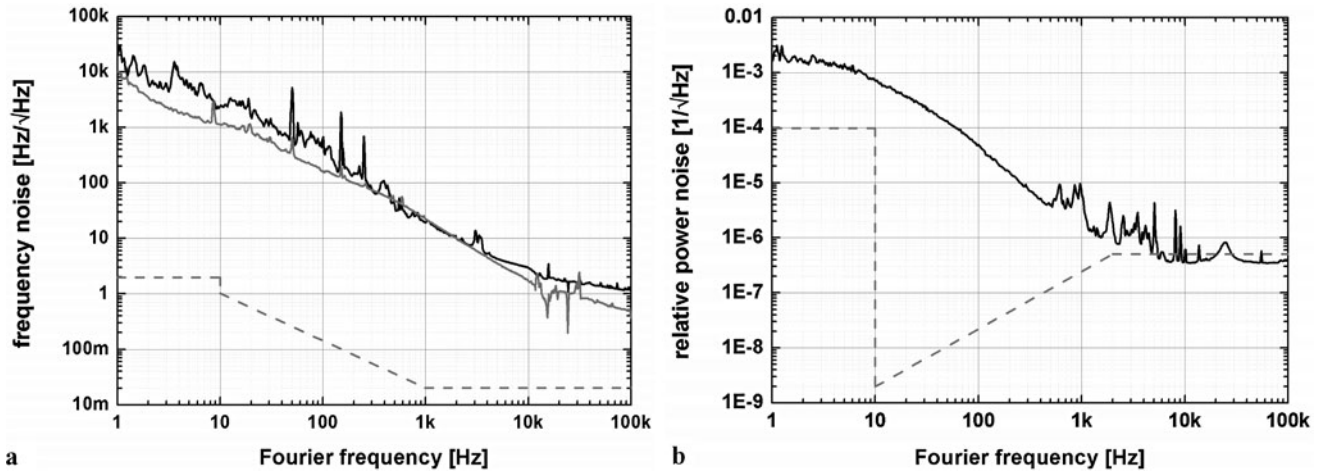

Fig. 12 (**a**) Frequency noise of the unstabilized laser: (*gray solid line*) typical frequency noise of a NPRO; (*dashed line*) Advanced LIGO requirements. (**b**) Relative power noise spectrum of the unstabilized laser output beam: (*dashed line*) Advanced LIGO requirements

bilization of the presented laser system is required. In order to minimize the loop gain requirements for the various stabilization stages, the output beam power and frequency fluctuations have to be kept at the lowest level possible. In Fig. 12(a), the frequency noise spectrum of the free-running injection-locked laser system at an output power of 220 W is shown. These measurements were taken with an optical diagnostic device developed by Kwee et al. [16]. It can be seen that the NPRO dominates the frequency noise of the 220 W beam and that the amplifier and the high-power oscillator add only approximately 5 dB of frequency noise. Hence we expect that a stabilization scheme similar to the one used for initial LIGO [5, 17] will allow us to reach the required frequency stability (dashed line in Fig. 12(a)).

For the characterization of the power noise of the laser system, two different measurements were performed. First of all, the peak-to-peak power fluctuations over 300 s of the output beam were determined. For this, the signal of a photodiode was sampled either with an oscilloscope or a Data Acquisition (DAQ) system. The oscilloscope was set to a sampling rate of approx. 26 kHz with the detector set to peak-detection while the DAQ system took samples at a rate of 125 kHz. In both cases, the relative peak-to-peak power noise of 7% set the requirement on the dynamic range of the power actuator used for the active stabilization.

The second measurement reveals the relative power fluctuations at different corresponding Fourier-frequencies (see Fig. 12(b)). To fulfill the requirements of the actively stabilized laser for the Advanced LIGO detector, the power variations at a frequency of 10 Hz have to be less than $2 \cdot 10^{-9}$ Hz$^{-1/2}$. Preliminary experiments of F. Seifert et al. [18] and P. Kwee et al. [19] showed that an active power stabilization is capable of reducing the power noise of a laser down to the required values.

6 Conclusions

In this article, we presented an injection-locked single-frequency laser with an output power of 220 W. Furthermore, it was possible to transmit 168 W through a non-confocal filter cavity resonantly locked to the fundamental mode. This is to our knowledge the highest output power of an injection-locked continuous-wave single-frequency laser, as well as the highest power in a pure TEM_{00} mode.

To ensure a stable long term operation of the laser system, a highly stable mechanical construction, including a straightforward thermal management, was developed. The implementation of a slow actuator with a large dynamic range for length control of the high-power oscillator cavity made it possible to demonstrate a stable single-frequency operation during an ambient temperature change of 2.5 K over a 40 h time period. Furthermore, within four continuous operation periods of 30 days each, separated by a few maintenance days for experiments, the laser system performed at nominal output power.

Even though the power level of the laser system was scaled above the 200 W level, the frequency and power noise could be kept in a range that can be actively stabilized to the requirements of advanced gravitational wave detectors. Hence the laser system presented in this paper is well suited as a light source for the next generation of gravitational wave detectors and other high precision experiments.

Acknowledgement This work was supported by the German Volkswagen Stiftung and the QUEST cluster of excellence at the Leibniz University Hannover.

References

1. B.P. Abbott, the LIGO Science Collaboration, Rep. Prog. Phys. **72**, 076901 (2009)
2. J. Abadie, VIRGO Collaboration, the LIGO Science Collaboration, LIGO document T0900499-v19 (2010). arXiv:1003.2481
3. B. Willke, Laser Photonics Rev. (2010). doi:10.1002/lpor.2009.00036
4. M. Frede, B. Schulz, R. Wilhelm, P. Kwee, F. Seifert, B. Willke, D. Kracht, Opt. Express **15**, 459 (2007)
5. B. Willke, K. Danzmann, M. Frede, P. King, D. Kracht, P. Kwee, O. Puncken, R.L. Savage Jr., B. Schulz, F. Seifert, C. Veltkamp, S. Wagner, P. Wessels, L. Winkelmann, Class. Quantum Gravity **25**, 114040 (2008)
6. M. Frede, R. Wilhelm, M. Brendel, C. Fallnich, F. Seifert, B. Willke, K. Danzmann, Opt. Express **12**, 3581 (2004)
7. M. Frede, R. Wilhelm, D. Kracht, C. Fallnich, Opt. Express **13**, 7516 (2005)
8. E. Khazanov, N.F. Andreev, A. Mal'shakov, O. Palashov, A.K. Poteomkin, A. Sergeev, A.A. Shaykin, V. Zelenogorsky, I.A. Ivanov, R. Amin, G. Mueller, D.B. Tanner, D.H. Reitze, IEEE J. Quantum Electron. **40**, 1500 (2004)
9. R.W.P. Drever, J.L. Hall, F.V. Kowalski, J. Hough, G.M. Ford, A.J. Munley, H. Ward, Appl. Phys. B **31**, 97 (1983)
10. R. Wilhelm, M. Frede, D. Kracht, Advanced solid-state photonics topical meeting Vancouver (CA). Paper MB19 (2007)
11. S. De Silvestri, P. Laporta, V. Magni, Opt. Commun. **65**, 373 (1988)
12. V. Magni, G. Valentini, S. De Silvestri, Opt. Quantum Electron. **23**, 1105 (1991)
13. Q. Lü, N. Kugler, H. Weber, S. Dong, N. Müller, U. Wittrock, Opt. Quantum Electron. **28**, 57 (1996)
14. B. Willke, N. Uehara, E.K. Gustafson, R.L. Byer, P.J. King, S.U. Seel, R.L. Savage Jr., Opt. Lett. **23**, 1704 (1998)
15. J.H. Poeld, LIGO document T0900616-v2 (2010). LIGO documents can be found at https://dcc.ligo.org/
16. P. Kwee, F. Seifert, B. Willke, K. Danzmann, Rev. Sci. Instrum. **78**, 073103 (2007)
17. R.L. Savage, P.J. King, S.U. Seel, Laser Phys. **8**, 679 (1998)
18. F. Seifert, P. Kwee, M. Heurs, B. Willke, K. Danzmann, Opt. Lett. **31**, 2000 (2006)
19. P. Kwee, B. Willke, K. Danzmann, Opt. Lett. **34**, 2912 (2009)